

Real-time radiography for observation of crack growth during GTA welding

F. T. Boateng^{1,2} · U. Ewert¹ · T. Kannengiesser^{1,2} · U. Zscherpel¹ · A. Griesche¹ · A. Kromm¹ · S. Hohendorf¹ · B. Redmer¹

Received: 18 January 2016 / Accepted: 26 April 2016 / Published online: 10 May 2016
© International Institute of Welding 2016

Abstract In situ crack detection in the mushy zone and the solid weld of a gas tungsten arc (GTA) weld using X-ray imaging during welding is a new research area for NDT inspection. Usually, NDT flaw detection is done after the complete solidification of the weld seam. In this paper, we present the use of real-time radiography with a minifocus X-ray source (YXLON X-ray tube Y.TU 225-D04) and a 75 µm pixel size digital detector array (Dexela 1512) for the acquisition of 2D radiographic images by a sequence of exposures with time intervals of 80 ms for hot crack detection during single pass bead-on-plate GTA welding of 3 mm thick plates of aluminium alloy AlMgSi (6060). An analysis of the crack distribution in the weld sample is conducted from the acquired 2D radiographs and its corresponding 3D volumetric reconstruction achieved by linear coplanar digital laminography. This in situ approach opens new possibilities in the field of hot crack research by having the direct information of both the crack initiation and growth and its correlation to the welding parameters.

Keywords (IIW Thesaurus) Hot cracking · Radiography · GTA Welding · Aluminium alloys · Real-time operations

Recommended for publication by Commission V - NDT and Quality Assurance of Welded Products

✉ F. T. Boateng
francis-twumasi.boateng@bam.de

¹ Federal Institute for Material Research and Testing (BAM), Berlin, Germany

² Otto-von-Guericke Universität Magdeburg, Institute of Materials and Joining Technology, Magdeburg, Germany

1 Introduction

Observation of crack formation and growth in the mushy zone as it undergoes solidification shrinkage in a steady weld process using X-ray has become a new research area for NDT inspection. Most NDT flaw inspections are usually done after the weld seam is completely solidified. The melting ranges of alloys are subjected to the risk of hot crack during its liquid to solid interface transition as a result of the dynamic weld pool flow phenomenon [1, 2]. Depending on the condition of hot crack formation and the location of occurrence, hot cracks can be subdivided into solidification cracks in the weld metal and liquation cracks in the heat-affected zone. One critical region where crack initiation and growth pertains is the liquidus-solidus interface of the weld pool (i.e. mushy zone). These flaws are common in alloy casting, and it is a pivotal issue defining the alloy's castability.

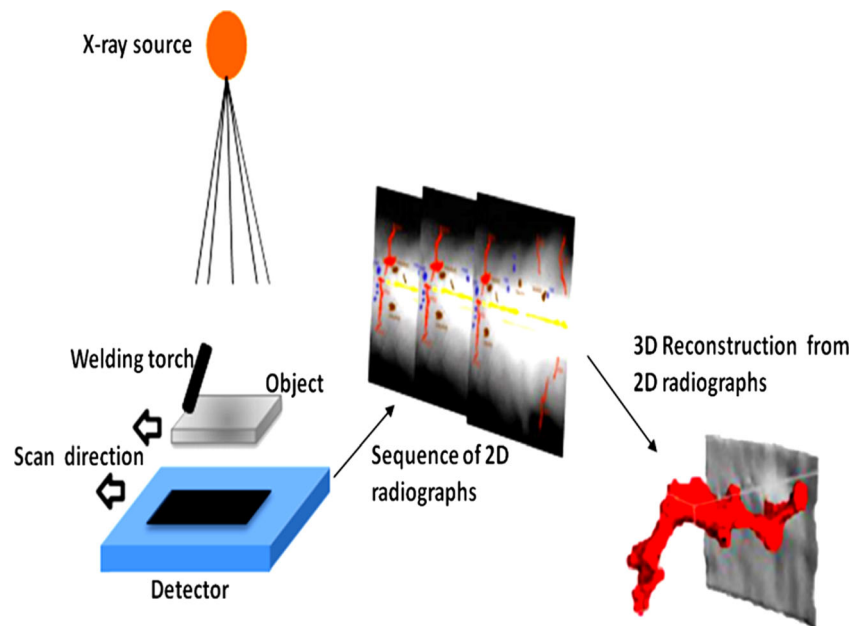
Other work like Helfen et al. [3] introduced the use of synchrotron radiation together with computer tomography for 3D inspections of cracks in composite polymers and alloys.

The main advantages of synchrotron radiation are the highly collimated, almost parallel beam and the photon flux, which are several orders of magnitude higher than conventional X-ray sources. On the other hand, the advantages of conventional X-ray tube-based setups are its easy accessibility and a large scanning area for cone beam-based systems. The latter allows also for a magnification of the object.

A conventional X-ray source was used for the observation of crack growth with linear coplanar digital laminographic techniques during GTA welding as illustrated in Fig. 1. The effect of welding parameters, such as welding speed on weld bead shape, will be discussed.

A laminographic imaging system was adapted to the experimental setup with a linear translation of detector and sample

Fig. 1 Schematic of the radiographic image acquisition with volume reconstruction



underneath a fixed X-ray source during welding. The synchronised motion of the sample and detector permits locating defects or flaws as the welded sample is penetrated from different angles [4]. The sample and detector are shifted at varying speeds and projections were taken in equidistant steps. The projections are weighted considering the nonlinear angle stepping from projection to projection and the variation of the beam length [5]. A high-pass filter is applied to achieve filtered back projection by averaging the related projection elements to generate a 3D image matrix. A cone beam correction algorithm is included in the laminographic reconstruction [4, 6].

2 Method

This section details the experimental setup used to acquire 2D radiographic images and 3D laminographic reconstructions.

2.1 Material and welding

A bead-on-plate weld was produced with a Lorch GTA welding system to stimulate hot cracking of an aluminium alloy plate AlMgSi (6060) of a 3 mm thickness in the dimension 150 mm × 150 mm. The alloy is used exemplarily for the reason of easy X-ray transmission and high cracking susceptibility. The chemical composition is listed in Table 1. The material was welded with argon as the shielding gas at a gas

Table 1 Chemical composition of AlMgSi (6060) weld sample (wt. %)

Si	Fe	Mn	Mg	Zn	Ni	Ti	Al
0.42	0.23	0.05	0.49	0.009	0.002	0.017	Balance

flow rate of 16 l/min. A tungsten electrode of 2.4 mm diameter was used. The electrode was positioned at an angle of 30° to the surface of the sample with an AC polarity (80 % negative, 20 % positive) and a frequency of 50 Hz.

A Photron Fastcam 1024PCI (model: 100KC) high-speed digital camera is used for the surface visualisation of the weld pool to compare the information from the surface to the information from the 3D model. It provides 1000 frames per second (fps) recording at 1024 × 1024 pixels.

Additionally, a web camera was used in the X-ray lab to survey the experiments from outside of the radiation protection room. Bead-on-plate welding was employed to ensure complete melting of the sample by applying the welding parameters as given in Table 2. The current was increased to compensate for higher welding speeds. At the beginning 2 s, welding at the edge of the sample without movement was chosen to ensure easy crack initialization and growth.

2.2 Acquisition of 2D radiographic image sequences

A 2D radiographic image sequence during sample weldment was generated using a YXLON X-ray tube Y.TU 225-D04 model with a focal spot size of 0.4 mm according to EN12543.

The experimental setup for digital radiography is shown in Fig. 2. The samples were placed on a linear motion

Table 2 Bead-on-plate welding parameters

Sample Number	BOP1	BOP2	BOP3	BOP4	BOP5
Voltage (U) in V	16	16	16	16	16
Current (I) in A	120	130	140	165	180
Speed (v) in mm s ⁻¹	2.3	2.8	3.6	5.3	8

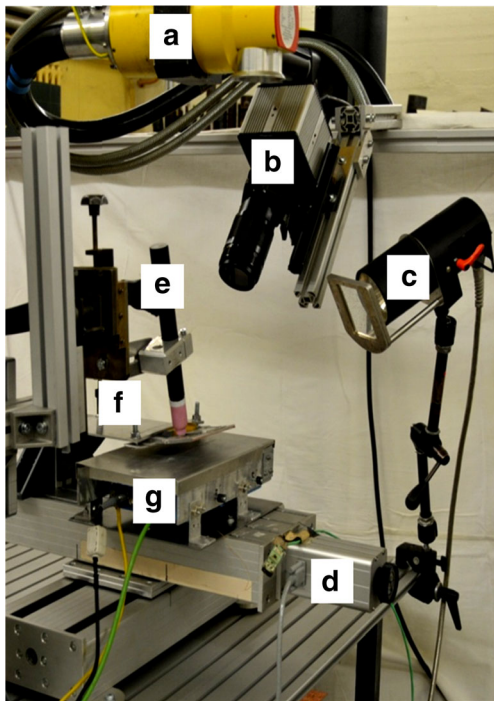


Fig. 2 Experimental setup with (a) X-ray tube, (b) high speed camera, (c) light source, (d) manipulator, (e) welding torch, (f) sample holder with sample and (g) DDA in the thermal shielding case

manipulator between the X-ray source and detector. Sequences of 2D radiographs are acquired during welding.

The specific settings of X-ray source voltage, current and radiograph acquisition time are presented in Table 3. A Digital Detector Array Dexela 1512 has been used for the acquisition of radiographs. It has a 75 μm pixel size and a CsI scintillator directly grown on the CMOS detector substrate. That results in a basic spatial resolution (SR_b) of 80 μm without binning. The detector has an ADC resolution of 14 bits per pixel at a readout mode of 10 frames per second.

The “Isee! Professional” acquisition software from Vision-in-X was used for 2D radiographic image acquisition and DDA calibration. The softwares “Isee! Professional” and “ImageJ” were used for image evaluation [7, 8].

Approximately 1500 sequential projections per scan at different angular positions during the welding process at different welding speeds and welding currents were acquired. The acquired sequential 2D projections were then reconstructed through a filtered shift average back projection algorithm. The VGStudio MAX software was used to facilitate further visualisation and analysis [9] as illustrated in Fig. 7.

Table 3 X-ray exposure parameters of the 2D image sequences

X-ray Voltage	X-ray Current	Focal spot	SDD	ODD	Frame number	Frame time
84 kV	4.1 mA	0.4 mm	426 mm	46 mm	1	0.04 s

The determination of the normalised signal-to-noise ratio (SNR_N) from the acquired 2D radiographic images was carried out on selected region of interests (ROIs) with a size of 20 × 55 pixels.

The linear grey values of the acquired 2D radiographs were evaluated. They are directly proportional to the radiation dose for determining the SNR, SR_b and SNR_N.

The basic spatial resolution SR_b of the image is related to the total image unsharpness measured with a duplex wire IQI according to ISO 19232-5:

$$SR_b^{image} = \frac{u_T}{2M}, \tag{1}$$

where u_T is the total detector unsharpness and M is the magnification.

u_T depends on both inherent unsharpness (u_i) of the detector and the geometric unsharpness (u_G) of the setup (see ISO 17636-2):

$$u_T = \sqrt{u_i^2 + u_G^2} \tag{2}$$

with $u_i = 2SR_b^{detector}$ and

$$u_G = \left(\frac{SDD}{f} - 1 \right) d$$

where f is the source to object distance, d is the focal spot size and SDD is the distance between the source and the detector.

The minimum permitted source to object distance (f_{min}) depends on the focal spot size (d) of the radiation source, the inherent unsharpness of the detector (u_i), the magnification M and thickness of the sample (t). If the inherent unsharpness of the detector is small, f_{min} is calculated as

$$f_{min} > 7.5 \frac{bd}{\sqrt[3]{t}} \tag{3}$$

according to testing class A of ISO 17636-2.

The unsharpness contribution of the detector (SR_b^{detector} divided by the magnification) used, must be smaller than the geometric image unsharpness (u_G/M) according to ISO 17636-2 testing class A of ISO 17636-2 (see Table B.13). The following values were determined:

$$f_{min} = 95.7\text{mm} < SOD = 380\text{mm}$$

$$\text{measured } SR_b^{image} = 80\mu\text{m}$$

Magnification was obtained from the relation below.

$$M = \frac{SDD}{SOD} = \frac{426\text{mm}}{380\text{mm}} = 1.12$$

The welded samples were radiographed according to the parameters stated in Table 3 and all radiographic images of the experimental samples were analysed. The normalised signal-to-noise ratio (SNR_N) and image quality values (IQI) of the welded sample were all determined.

2.3 Image quality parameters

The minimum detectable crack width with X-ray radiography depends mostly on the inner unsharpness of the detector. Parameters for detail visibility in radiography are the contrast-to-noise ratio (CNR) and the spatial basic resolution (SR_b). The CNR can be determined from the SNR as a function of exposure dose considering the effective attenuation coefficient, μ_{eff} [5]:

$$\frac{CNR}{\Delta t} = SNR * \mu_{eff} \tag{4}$$

where $\Delta t \ll t$

The pixel size and unsharpness of the digital detector array are considered by the concepts of normalised SNR:

$$SNR_N = \frac{SNR * 88.6 \mu m}{SR_b} \tag{5}$$

The SNR_N depends on the radiation energy and exposure conditions. This influences the image quality required for visibility of IQIs and flaws.

3 Discussion

3.1 2D radiographic image evaluation

In Fig. 3, we show the comparison of the surface photograph and the 2D radiographic image of the welded sample. The quality of a radiographic image can be assessed in terms of image sharpness, image contrast and image noise. A standardised wire Image Quality Indicator (IQI acc. to 19232-1) is typically included in the image to determine image quality of the radiographs not shown here. The use of an IQI is to indicate the sensitivity of the technique and equipment used. Single and duplex wire IQIs are the mostly used IQIs. The single wire IQI is used to check the contrast sensitivity achieved and the duplex wire IQI is used to measure the basic spatial resolution of the image. The duplex wire IQI consists of 13 wires pairs of platinum with various diameters embedded in a rigid plastic block. The number of wire pairs that can be seen separated indicates the unsharpness. The first resolved wire pair is determined by a profile function according to ASTM E 2002-15 for determination of SR_b .

The single wire set consists of a series of straight wires of the same material as the sample, with different diameters. The smallest wire, which is detected at least 10 mm in the base material, determines the contrast sensitivity.

The measured SNR_N in the digital radiographs depends on the frame number, the X-ray tube current and the SDD for a given exposure time. The maximum image quality is limited

Starting edge (a 2s welding without movement for crack initialisation and growth)

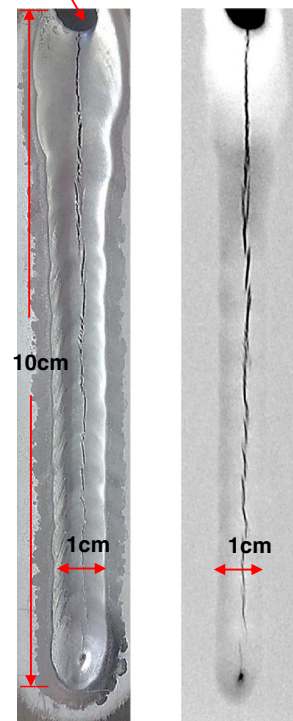


Fig. 3 Comparison of photograph (left) and a 2D radiographic projection image of the weld (right)

due to the influence of photon noise introduced by the calibration of the detector, which limits the image quality independently of the exposure conditions as seen in Fig. 4.

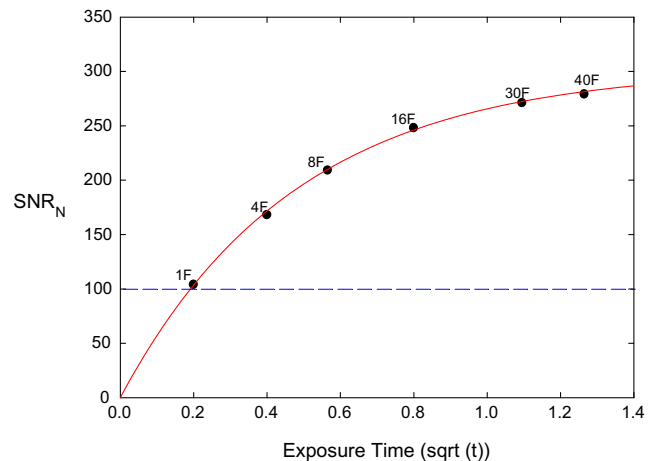


Fig. 4 SNR_N as a function of exposure time in seconds (solid line) for various frame numbers F. The dashed line denotes the minimal requirement for this experiment

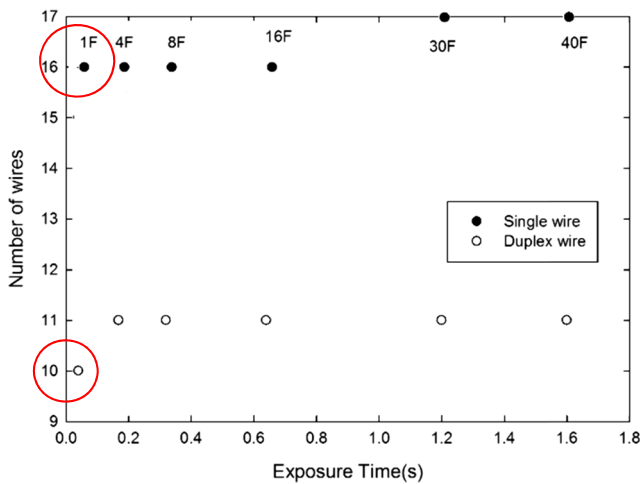


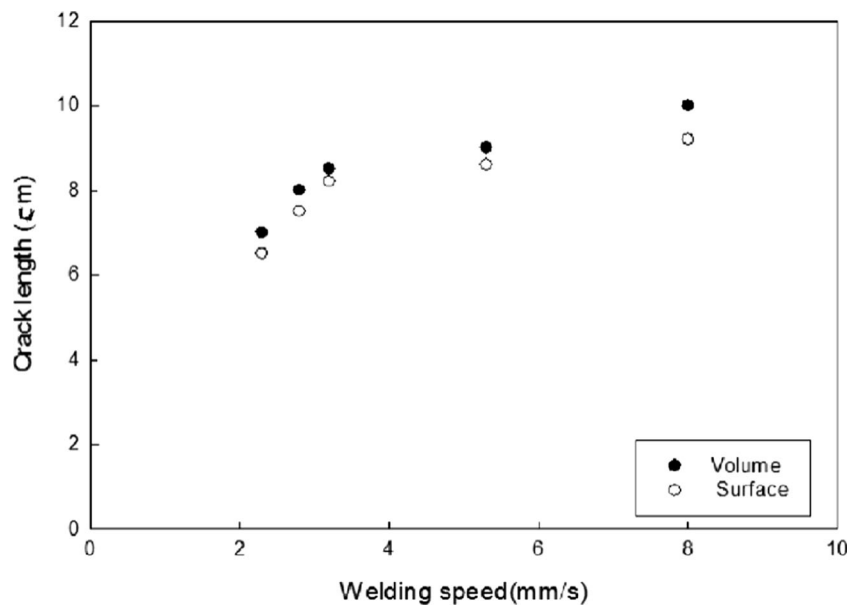
Fig. 5 Single wire sensitivity and duplex wire separation for 1 to 40 frames

Table 4 The required minimum image quality values (IQI) for a 3-mm AlMgSi (6060)

IQI requirements of ISO 17636-2	Testing class A	Testing class B
Single wire	W16	W17
Duplex wire	D10	D13

The achieved contrast sensitivity and image unsharpness IQI values are shown in Fig. 5. This shows that the minimum requirements of testing class A were achieved already for an exposure time of 40 milliseconds (1 frame) according to ISO 17636-2, see Table 4: The requirements

Fig. 6 Comparison of crack length in a volume and on surface of the weld sample



for testing class B according to ISO 17636-2, cannot be fulfilled with the chosen detector and exposure conditions, even when using compensation principle II according to ISO 17636-2. This requires to detect W19 instead of W17, when only D11 is achieved instead of D13 as required for testing class B for a 3-mm material. This requires an integration time much longer than the 2 s as shown in Fig. 5, i.e. testing class B were not achieved for real time applications.

The basic spatial resolution of the image obtained for D10 is 100 μm (see table B.13 in ISO 17636-2).

The cumulative crack length is a common measure for the cracking susceptibility in a hot cracking test [10, 11]. Often, this is performed just on the surface of the sample. Nevertheless, cracks can be situated in the volume invisible for surface inspection. In this case, the 2D radiographic images allow for evaluation taking into account the whole thickness of the welded sample. The calculated crack lengths for varying samples were compared as shown in Fig. 6. The crack lengths found in the volume show slightly higher values compared to the surface. Increasing the welding speed produces more cracks in the sample.

3.2 Time resolved observation of crack growth

Figure 7 shows the time-dependent crack growth during welding in time intervals of 20 s of the 3-mm AlMgSi 6060 plate. The crack is visible in a certain distance from the welding torch and it is growing in dependence on the

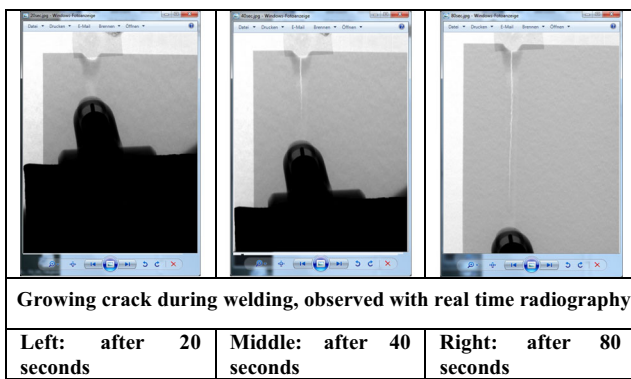


Fig. 7 Growing crack during welding, observed with real time radiography

welding progress. Further investigations are planned for quantitative characterization of the crack growth in dependence on the welding conditions.

3.3 3D laminography

In Fig. 8, the reconstruction of the weld seam of the projected 2D radiographic image sequence has shown the capabilities for 3D imaging. The linear coplanar scanning principle yields several advantages such as the

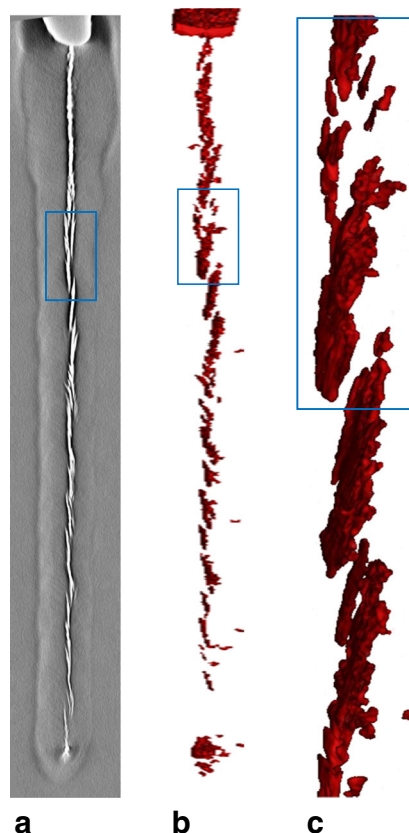


Fig. 8 Comparison of (a) high-pass filtered slice of the 3D laminographic reconstruction and (b) 3D representation of reconstruction volume at a 1-mm depth. (c) Enlarged volume of (b)

application of different radiation angles to obtain 3D data. The multi-angle technique provides sufficient information for a 3D reconstruction of the weld. The reconstruction is based on a modified filtered shift average algorithm. This algorithm is a typical analysis method for both qualitative and quantitative evaluation of the different structures, including crack depth [12]. The thickness of the sample plate and the inner shape of the crack can be reconstructed with the same data set of projections. This also provides non-destructively cross sections as an alternative to metallographic sectioning.

A 3D reconstruction allows a more accurate observation of the central zone of hot cracks. The crack shape and depth at the centre of the fusion zone, which can only be guessed from 2D radiographs, are clearly visible.

4 Conclusions

A fast time resolved digital X-ray radiography technique was developed for crack growth observation. A time resolution of 40 ms per frame and an acquisition speed of 10 frames per second could be achieved during welding. The time resolved digital radiography permits the observation of growing cracks. The frames were taken in class A quality of ISO 17636-2. The multi angle linear coplanar laminography permits the depth resolution of cracks in the tested samples of the aluminium alloy of a 3-mm thickness in the dimension 150 mm × 150 mm. Cumulative crack lengths could be determined at surface and subsurface in depths. The application of a modified filtered shift average back projection method for 3D reconstruction provided sufficient image quality with short reconstruction time for the depth dependent evaluation of the results.

Acknowledgments The authors want to thank K.U. Thiessenhusen, C. Bellon, M. Grunwald, D. Walter, A. Deresch and M. Tschaikner of Division 8.3 Radiological Methods, A. Hannemann of Division 9.4 Weld Mechanics and D. Stock, M. Richter and K. Scheideck of Division 9.3 Welding Technology of Bundesanstalt für Materialforschung und-prüfung (BAM) for their support.

References

1. Kannengießer T, Bollinghaus T (2014) Hot cracking test—an overview of present technologies and application. *Weld World Springer* 58(3):397–421
2. Ewert U, Zscherpel U, Heyne K, Jechow M, Bavendiek K (2012) Image quality in digital industrial radiography. *Mater Eval* 70(8): 955–964, 10p
3. Helfen L et al (2011) On the implementation of computed laminography using synchrotron radiation. *Rev Sci Instrum* 82(6): 063702
4. Gondrom S, Schropfer S (1999) Digital computed laminography and tomosynthesis- functional principles and industrial

- applications. International Symposium on Computerized Tomography for Industrial Applications and Image Processing in Radiology, Berlin, Germany Proceedings BB 67-CD published by DGZfP
5. Ewert U, Jaenisch G-R, Zscherpel U, Osterloh K, Redmer B (2013) Chapter “Industrial radiology” in “Handbook of technical diagnostics”. Springer, p 221–247
 6. Thiessenhusen KU, Ewert U, Redmer B, Bavendiek K (2011) Geometric corrections in coplanar translational Laminography, DIR 2011, Conference proceedings, Berlin
 7. Isee! Professional website (<http://www.vision-in-x.com/en/home.html>)
 8. ImageJ website (<http://imagej.nih.gov/ij/>)
 9. VGStudio website (<http://www.volumegraphics.com>)
 10. Schempp P, Cross CE, Pittner A, Rethmeier M (2013) Influence of grain size on mechanical properties of aluminium GTA weld metal. *Weld World* 57(3):293–304
 11. Ghosh A et al (2011) Assessment of heat affected zone of submerged arc welding process through digital image processing. *Procedia Eng* 10:2782–2785
 12. Redmer B, Robbel J, Ewert U, Vengrinovich VV (2002) Mechanised weld inspection by tomographic computer-aided radiometry (TomoCAR). *Insight* 44(9):564–567